

Highlights

WHU-PCPR: A cross-platform heterogeneous point cloud dataset for place recognition in complex urban scenes

Xianghong Zou, Jianping Li, Yandi Yang, Weitong Wu, Yuan Wang, Qiegen Liu, Zhen Dong

- A cross-platform heterogeneous point cloud dataset for place recognition is established.
- A comprehensive benchmark for place recognition is conducted on the proposed dataset.

WHU-PCPR: A cross-platform heterogeneous point cloud dataset for place recognition in complex urban scenes

Xianghong Zou^a, Jianping Li^{b,*}, Yandi Yang^c, Weitong Wu^d, Yuan Wang^e, Qiegen Liu^{f,*} and Zhen Dong^{g,h}

^aSchool of Advanced Manufacturing, Nanchang University, Nanchang, 330031, China

^bSchool of Electrical and Electronic Engineering, Nanyang Technological University, 50 Nanyang Avenue, 639798, Singapore

^cDepartment of Geomatics Engineering, University of Calgary, Calgary, T2N 1N4, Canada

^dSchool of Earth Sciences and Engineering, Hohai University, Nanjing, 211100, China

^eSchool of Geography and Environment, Jiangxi Normal University, Nanchang, 330022, China

^fSchool of Information Engineering, Nanchang University, Nanchang, 330031, China

^gState Key Laboratory of Information Engineering in Surveying, Mapping and Remote Sensing, Wuhan University, Wuhan, 430079, China

^hHubei Luojia Laboratory, Wuhan, 430079, China

ARTICLE INFO

Keywords:

LiDAR Point Cloud Dataset

Place Recognition

Cross-platform

Heterogeneous

Benchmark

ABSTRACT

Point Cloud-based Place Recognition (PCPR) demonstrates considerable potential in applications such as autonomous driving, robot localization and navigation, and map update. In practical applications, point clouds used for place recognition are often acquired from different platforms and LiDARs across varying scene. However, existing PCPR datasets lack diversity in scenes, platforms, and sensors, which limits the effective development of related research. To address this gap, we establish WHU-PCPR, a cross-platform heterogeneous point cloud dataset designed for place recognition. The dataset differentiates itself from existing datasets through its distinctive characteristics: 1) cross-platform heterogeneous point clouds: collected from survey-grade vehicle-mounted Mobile Laser Scanning (MLS) systems and low-cost Portable helmet-mounted Laser Scanning (PLS) systems, each equipped with distinct mechanical and solid-state LiDAR sensors. 2) Complex localization scenes: encompassing real-time and long-term changes in both urban and campus road scenes. 3) Large-scale spatial coverage: featuring 82.3 km of trajectory over a 60-month period and an unrepeatable route of approximately 30 km. Based on WHU-PCPR, we conduct extensive evaluation and in-depth analysis of several representative PCPR methods, and provide a concise discussion of key challenges and future research directions. The dataset and benchmark code are available at <https://github.com/zouxianghong/WHU-PCPR>.

1. Introduction

Place Recognition (PR) determines one's approximate location within a pre-built map based on scene similarity, serving as an effective coarse localization technique and a fundamental component for global localization. It offers considerable application potential in fields such as autonomous driving (Häne et al., 2017), robot localization and navigation (Wang et al., 2021; Li et al., 2025), multi-robot cooperative localization and mapping (Yuan et al., 2017; Li et al., 2025), map update (Kim and Kim, 2020), augmented reality (Chi et al., 2022), and counter-terrorism rescue operations (Bin Shamsudin et al., 2017). LiDAR (Light Detection and Ranging), as an important 3D vision sensor, is less susceptible to influences such as lighting and weather conditions compared to cameras, while providing accurate geometric, shape, and scale information, enabling Point Cloud-based Place Recognition (PCPR) to achieve

stronger environmental adaptability (Li et al., 2019; Yang et al., 2024).

In practical applications, point clouds used for PR are often acquired from different platforms and LiDARs (Zou et al., 2023). Due to differences in the motion patterns, observation modes, and applicable ranges of the platforms, as well as variations in the LiDAR sensors' field of view, channel count, scanning pattern, frequency, accuracy, and measurement range, the collected point clouds exhibit significant discrepancies in accuracy, density, noise, coverage, and point distribution patterns, i.e., domain gaps (Qingqing et al., 2022; Yang et al., 2024). Such point clouds are thus termed heterogeneous point clouds. Taking map update as an example, a common practice is to first collect high-precision point clouds using Mobile Laser Scanning (MLS) systems as the base map, followed by later updates with point clouds acquired by low-cost Portable Laser Scanning (PLS), such as helmet-mounted (Li et al., 2023, 2024). Before updating the map, the PLS data must be aligned to the MLS coordinate system. Global Navigation Satellite System (GNSS) provides the simplest and most direct means for this alignment. However, in GNSS-denied environments such as urban canyons, obtaining reliable positional information via GNSS becomes challenging (Li et al., 2026). Thus, research on PR for heterogeneous point clouds is essential.

* This research was supported by the National Natural Science Foundation Project (No.42201477, No.42501567), Jiangxi Provincial Natural Science Foundation (No.20252BAC200598, No.20242BAB21014, No.20252BAC240107)

*Corresponding author

 ericxhzhou@ncu.edu.cn (X. Zou); jianping.li@ntu.edu.sg (J. Li); yandi.yang@ucalgary.ca (Y. Yang); weitongwu@hhu.edu.cn (W. Wu); wangyuanwu@jxnu.edu.cn (Y. Wang); liuqiegen@ncu.edu.cn (Q. Liu); dongzhenwu@whu.edu.cn (Z. Dong)

Existing PCPR methods can be mainly categorized into two types: handcrafted feature-based and deep learning (DL)-based. The former relies on manually designed rules to extract features for PR, typically tailored to specific platforms and sensor types (Kim and Kim, 2018; He et al., 2016). The latter utilizes deep neural networks to extract global features (Hui et al., 2021; Komorowski, 2021). These DL-based methods, though mainstream, are prone to severe overfitting on public datasets (Zhang et al., 2024). Besides, some reranking techniques have been introduced to enhance the PR performance (Zhang et al., 2022; Vidanapathirana et al., 2023). Datasets play a crucial role in advancing PCPR techniques, especially for DL-based methods. However, existing PCPR datasets lack sufficient diversity in scenes, platforms, and LiDAR types to meet current research demands. 1) *Limited scene diversity*: Most datasets are collected in well planned cities with short time spans and minimal scene changes. For example, Oxford Radar RobotCar dataset (Barnes et al., 2020) is collected in the highly developed Oxford urban area within 1 month, where the roads are clean and the scene changes are minimal. 2) *Limited platforms and LiDAR types*: Point clouds collected from different platforms and LiDARs exhibit significant domain gaps. While most datasets are only collected by vehicle-mounted laser scanning systems, such as KITTI Odometry (Geiger et al., 2012) and HeLiPR (Jung et al., 2023). Most datasets are collected only with mechanical LiDARs, such as NCLT (Carlevaris-Bianco et al., 2016) and Wild Place (Knights et al., 2023). 3) *Limited spatial coverage*: For example, the well-established Oxford RobotCar dataset (Maddern et al., 2017) consists of over 100 repeated traversals along the same trajectory, which extends only approximately 10 km in length, resulting in limited spatial coverage. Therefore, there is an urgent demand for a heterogeneous PCPR dataset that encompasses diverse scenes, platforms, and LiDARs, providing essential data support for advancing research in this field.

In this paper, we establish WHU-PCPR, a cross-platform heterogeneous point cloud dataset designed for PR. The dataset is collected across urban and campus roads in Wuhan using high-precision vehicle-mounted laser scanning (MLS) systems and a portable helmet-mounted laser scanning (PLS) system, covering a total length of 82.3 km. Captured over a span of 60 months, it incorporates complex real-world scenes and diverse LiDARs, thereby reflecting practical challenges in PCPR and supporting further research. Using WHU-PCPR, we experimentally evaluate several representative PCPR methods, analyze current limitations and key challenges, and suggest potential directions for future work.

Our **main contributions** are as follows:

- (1) A cross-platform heterogeneous PCPR dataset (WHU-PCPR) is established. It features cross-platform heterogeneous point clouds, complex localization scenes, and extensive spatial coverage, spanning a trajectory length of 82.3 km and a temporal duration of 60 months, presenting substantial challenges for PCPR.

- (2) A comprehensive benchmark for PCPR is conducted on WHU-PCPR, providing researchers with an intuitive understanding of the field's development level and existing problems. Specifically, existing retrieval methods need major improvements in generalizability across scenes, platforms, and sensor types, and in robustness to viewpoint variations. Reranking techniques can effectively enhance initial retrieval results.

The remainder of this paper is structured as follows. In section 2, we review the existing datasets and methods for PCPR. In section 3, we describe the proposed cross-platform heterogeneous point cloud dataset for PR. In section 4, we present detailed benchmark results for existing methods on WHU-PCPR. In section 5, we summarize the challenges and discuss possible future directions. In section 6, we give our conclusion.

2. Related works

2.1. Public PCPR datasets

PCPR is a highly complex task that encompasses diverse scenes, sensor configurations, and deployment platforms. In practical applications, it is essential to consider factors such as generalizability, viewpoint robustness, scene changes, computational efficiency, and storage efficiency. Furthermore, achieving efficient and reliable retrieval requires the integration of multiple technologies, including PR, reranking, and continual learning. Consequently, the advancement of these technologies necessitates the support of rich and diverse public datasets.

A range of datasets are commonly employed for PCPR research, including KITTI Odometry (Geiger et al., 2012), NCLT (Carlevaris-Bianco et al., 2016), Oxford RobotCar (Maddern et al., 2017), and others. Among these, KITTI Odometry is a classic benchmark in autonomous driving. The Oxford RobotCar and In-house datasets were notably pioneered in PointNetVLAD, the first deep learning-based PCPR method. Others address specific niches: Wild Place (Knights et al., 2023) is the first focused on unstructured natural scenes, and HeLiPR (Jung et al., 2023) utilizes a MLS system equipped with multiple types of LiDARs. However, a review of these datasets (detailed in Table 2) reveals a common constraint: most are constructed from repeated data collection runs using the same equipment in similar urban environments. Consequently, the scene diversity and the variety of acquisition platforms and sensors are significantly limited. This homogeneity risks creating a misleading impression that current PCPR methods perform exceptionally well, masking their potential shortcomings in handling real-world complexity.

2.2. PCPR methods

Existing PCPR methods include two steps: retrieval and reranking (Vidanapathirana et al., 2023). The former performs initial PR using either handcrafted features or deep learning-based features. The latter employs techniques like

Table 1
Commonly used public datasets for PCPR.

Dataset	Year	Scene	Platform	LiDAR	Sequence	Time span (month)	Site	Length (km)
Ford Campus (Pandey et al., 2011)	2011	outdoor	vehicle	Velodyne HDL-64E	-	1	Michigan, USA	-
KITTI Odometry (Geiger et al., 2012)	2012	outdoor	vehicle	Velodyne HDL-64E	22	-	Karlsruhe, Germany	39.2
NCLT (Carlevaris-Bianco et al., 2016)	2016	indoor + outdoor	robot	Velodyne HDL-32E	27	15	Michigan, USA	147.4
Oxford RobotCar (Maddern et al., 2017)	2017	outdoor	vehicle	SICK LMS-151	133	19	Oxford, UK	1010.5
In-house (Uy and Lee, 2018)	2018	outdoor	vehicle	Velodyne HDL-64E	15	-	-	108.0
Apollo SouthBay (Lu et al., 2019)	2019	outdoor	vehicle	Velodyne HDL-64E	-	-	San Francisco, USA	380.5
HKUST (Lin and Zhang, 2019)	2019	outdoor	handheld	Livox Mid-40 / Mid-100	-	-	HongKong	-
Complex Urban (Jeong et al., 2019)	2019		vehicle	Velodyne VLP-16	19	-	Korea	190.0
MulRan (Kim et al., 2020)	2020	outdoor	vehicle	Ouster OS1-64	12	2	Seoul, Korea	123.0
Ford Multi-AV (Agarwal et al., 2020)	2020	outdoor	vehicle	Velodyne HDL-32E	-	3	Michigan, USA	198.0
Oxford Radar RobotCar (Barnes et al., 2020)	2020	outdoor	vehicle	Velodyne HDL-32E	32	1	Oxford, UK	280.0
USyd (Zhou et al., 2020)	2020	outdoor	vehicle	Velodyne VLP-16	52	13	Sydney, Australia	-
ALITA (Yin et al., 2022)	2022	outdoor	vehicle	Velodyne HDL-64E	-	-	Pittsburgh, USA	156.0
KITTI-360 (Liao et al., 2022)	2022	outdoor	vehicle	Velodyne HDL-64E / SICK LMS 200	9	-	Karlsruhe, Germany	73.7
HAOMO (Ma et al., 2022)	2022	outdoor	vehicle	HESAI PandarXT 32	5	1	Beijing, China	-
Wild Place (Knights et al., 2023)	2023	outdoor	handheld	Velodyne VLP-16	8	14	Brisbane, Australia	32.9
Boreas (Burnett et al., 2023)	2023	outdoor	vehicle	Velodyne Alpha-Prime	44	12	Toronto, Canada	350.0
Pohang (Chung et al., 2023)	2023	outdoor	boat	Ouster OS1-32	5	-	Pohang, Korea	45.0
				Ouster OS2-128				
				Velodyne VLP-16				
				Livox Avia				
				Aeva Aeries II				
Wuhan-HPC (ours)	2025	outdoor	vehicle + helmet	Surveying grade LiDAR Livox Avia / Mid70 / Mid360	6	60	Wuhan, China	82.3

query expansion (Chum et al., 2007) and point cloud registration (Zhang et al., 2022) to refine initial retrieval results through additional information, and it's an optional step.

Retrieval. These methods can be categorized into hand-crafted feature-based and deep learning-based. *Handcrafted feature-based* methods extract features for PR based on manual rules, including projection, histogram, and so on. Projection-based methods convert point clouds into 2D images for feature extraction. Scan Context (Kim and Kim, 2018), Skyline Context (Liang et al., 2020), and PGHCI (Xu et al., 2022) convert point clouds into bird's eye view (BEV) images. M2DP (He et al., 2016) projects point clouds onto six different planes and calculates the number of points within each plane's fan-shaped grid. Histogram-based methods divide the point cloud into grids to build statistical histograms. Delight (Cop et al., 2018) divides the point cloud into spherical grids and calculates intensity distributions. Loam-livox (Lin and Zhang, 2019) divides the point cloud into regular grids and calculates the number of grids with different principal directions. NDT-histogram (Magnusson et al., 2009; Röhling et al., 2015) employs spherical grids, classifying them into three categories based on eigenvalues. Other methods directly extract features from point clouds for PR. Bosse and Zlot (2013) utilizes 3D point features and geometric consistency for loop closure detection. SegMatch (Dubé et al., 2017) performs ground removal and segmentation, followed by feature extraction via manual rules. In summary, most handcrafted methods rely on manual rules, typically only applicable to specific platforms and LiDARs, and are sensitive to viewpoint variations, occlusions, and noises.

Deep learning-based methods utilize deep networks to extract global features, and can be divided into three categories: point-based, voxel-based, and projection-based. Point-based methods directly extract global features from raw point clouds. The pioneering PointNetVLAD (Uy and Lee, 2018) combines PointNet (Qi et al., 2017) and NetVLAD for global feature extraction. PPT-Net (Hui et al., 2021) enhances feature extraction capabilities with Edge-Conv and Transformer. On this basis, PatchAugNet (Zou et al., 2023) achieves heterogeneous PCPR through patch feature augmentation and adaptive pyramid feature aggregation. LAWS (Xie et al., 2024) treats PR as a classification task and eliminates classification ambiguity through two spatial partitioning patterns. Voxel-based methods extract features from voxelized point clouds. MinkLoc3D (Komorowski, 2021) employs sparse convolution and feature pyramid networks, followed by GeM pooling (Radešović et al., 2018) and hard negative mining to achieve strong performance. Its extension, EgoNN (Komorowski et al., 2021), extracts local and global features for joint PR and pose estimation. LoGG3D-Net (Vidanapathirana et al., 2022) obtains more repetitive global features through sparse point-voxel convolution. Projection-based method extracts features from 2D projection images. OverlapNet (Chen et al., 2021) projects point clouds to range images and uses a Siamese network to directly regress overlap and yaw angle. Built upon Scan Context, SCI-localization (Kim et al., 2019) converts PR into a classification task. BEVPlace (Luo et al., 2023) utilizes group convolution to extract rotation-equivariant features from BEV images, then obtains rotation-invariant features through NetVLAD. In

summary, while DL-based methods generally outperform handcrafted counterparts, they require large-scale geotagged data for training. Their transferability across diverse scenes and LiDARs, as well as robustness to scene changes, remain key challenges for improvement.

Reranking. In challenging scenes, single retrieval consistently struggles with performance. It's necessary to adjust the initial retrieval results using additional information, and this step is called reranking. The concept of reranking originates from the field of information retrieval and has subsequently been adopted and developed in areas such as image retrieval (Joshi et al., 2014), object retrieval (Tolias et al., 2015), and shape retrieval (Bai et al., 2017). However, relevant methods in the field of PCPR remain scarce. Reranking methods for PCPR can be categorized into two types: query expansion and geometric consistency.

Query expansion utilizes the features of the retrieved top k items to update the feature of query item for reranking, such as AvgQE (Chum et al., 2007) and AlphaQE (Radešović et al., 2018). These methods can jump out from the initial retrieval results and discover more correct items, but they require traversing the entire feature database. Methods based on geometric consistency primarily leverage registration scores to rerank the top k items, such as Rank-PointRetrieval (Zhang et al., 2022) and SGV (Vidanapathirana et al., 2023). These approaches are computationally intensive and do not consider the semantic and spatial relationships among the retrieved top k items. In summary, existing reranking methods suffer from both noise sensitivity and computational efficiency. Among them, methods based on geometric consistency tend to be more reliable.

3. Construction of WHU-PCPR dataset

3.1. Data collection

WHU-PCPR dataset is collected in the urban area of Wuhan, China using high-precision MLS systems and portable PLS systems, as shown in Fig. 1. This section details the collection process.

Acquisition area. WHU-PCPR comprises two distinct regions: Hankou and WHU, as shown in Fig. 1. Hankou data is collected along typical urban thoroughfares in Wuhan, including Jiefang Road, Yanjiang Road, and Zhongshan Park. The scenes feature dense high-rise buildings, overpasses, street trees, and dynamic objects. WHU data covers areas within Wuhan University, including computer science (CS) college and Information (Info) campus. These scenes are characterized by confined spaces, dense vegetation, and highly unstructured terrain. Over the 60-month period, some areas in both Hankou and WHU show significant changes.

Acquisition equipments. WHU-PCPR collects heterogeneous point clouds with survey-grade MLS systems and low-cost portable PLS systems, as shown in Fig. 3. The MLS systems (Hi-Target HiScan-VUX and CHCNAV Alpha 3D) are equipped with high-precision positioning and orientation systems as well as single-beam, high-frequency mechanical LiDARs, and the collected point clouds are of high precision,

high density, and wide coverage. The PLS system, designated WHU-Helmet (Li et al., 2023), is equipped with a semi-solid state LiDAR, i.e. Livox Mid70, Avia or Mid360. Solid-state LiDARs use non-repetitive scanning and typically have a shorter range, resulting in point clouds with lower accuracy, lower density, and reduced coverage.

Statistics of WHU-PCPR. WHU-PCPR comprises 6 sequences spanning a total trajectory length of 82.3 km over 60 months. Spatially, the dataset comprises 38,616 submaps, with 31,466 from MLS and 7,150 from PLS. Correspondingly, it covers 82.3 km of trajectories, with 30.81 km from MLS and 51.49 km from PLS. Temporally, the Hankou subset spans 60 months, while the WHU subset covers 20 months. A detailed summary is provided in Table 2.

3.2. Data preprocessing

The preprocessing of our dataset includes data alignment, submap construction, and data splitting.

Data alignment. The position accuracy of the MLS trajectory is exceptionally high, whereas the initial PLS trajectory is derived using FAST-LIO2 (Xu et al., 2022). In this paper, PLS point clouds are first segmented into blocks, followed by manual alignment with MLS point clouds using CloudCompare. The average registration accuracy of the multi-phase point clouds is 0.28 m, which meets the experimental requirements. More details refer to Fig. 2.

Submap construction. Circular submaps with a 30-meter radius are generated at 2-meter intervals along each trajectory. Before submap construction, dynamic objects are removed from the PLS point clouds using Octomap (Hornung et al., 2013). For each submap, ground points are then filtered out via cloth simulation filtering (Zhang et al., 2016), and the remaining points are downsampled to 4096 using farthest point sampling. Finally, the coordinates of all points are normalized to the range [-1, 1].

Data splitting. The dataset is partitioned using rectangular regions along the x/y axes. For sequences Hankou 1&2, submaps within specific rectangles are designated as the test set, while the rest form the training set, resulting in an approximate 5:1 train-test ratio. All submaps from the remaining sequences are used for testing. In the training set, submaps are defined as positive pairs when their centers are within 15 m, and as negative pairs when the distance exceeds 60 m. During testing, a retrieval is considered successful if the retrieved submap is within 30 m of the query.

3.3. Characteristics of WHU-PCPR

As shown in Fig. 3, the WHU-PCPR dataset exhibits three key characteristics:

- (1) **Cross-platform heterogeneous point clouds:** First, the dataset is collected using laser scanning systems from two distinct platforms, aligning more closely with practical applications where high-precision, high-cost laser scanning systems are deployed in early stages and portable, low-cost systems are adopted in later stages. The motion ranges and patterns of the different platforms differ significantly. Second, different platforms



Fig. 1. Overview of WHU-PCPR dataset. A, B, and C represent three typical scenes.

Table 2

Detailed description of WHU-PCPR dataset.

Region	Phase	Scene	Platform	LiDAR	Acquisition time	Length (km)	Submap: Train/Test
Hankou	1	Urban road	Vehicle	Hi-Target HiScan-VUX	2019-12-11, 2020-03-20, 2020-03-22	24.64	10329 / 1563
	2		Helmet	Livox Avia	2022-08-23	15.42	5467 / 1594
	3		Helmet	Livox Mid360	2023-07-21, 2023-07-23, 2024-12-13	27.51	12513 / 0
WHU	1	Campus road	Vehicle	CHCNAV Alpha3D	2021-11-20	6.17	2995 / 0
	2		Helmet	Livox Avia / Mid70	2021-11-12, 2022-07-29	4.06	2023 / 0
	3		Helmet	Livox Mid360	2023-07-18	4.49	2132 / 0

often carry different types of LiDARs, varying in terms of measurement range, accuracy, scanning frequency, and scanning pattern. Due to the above reasons, the collected point clouds exhibit significant differences in accuracy, density, coverage, and noise levels. These differences are more pronounced compared to the another heterogeneous dataset HeLiPR (Jung et al., 2023).

- (2) **Complex localization scenes:** First, campus roads typically exhibit dense vegetation, few artificial structures, and highly unstructured surroundings, while urban roads are marked by abundant street trees, tall buildings, overpasses, and dynamic objects like vehicles and pedestrians. Second, the three-phase data collection spans a five-year period, during which certain scenes have undergone substantial changes, such as buildings and trees.
- (3) **Large-scale spatial coverage:** In contrast to the widely recognized Oxford RobotCar dataset, which has a unpeated route of about 10 km, the WHU-PCPR dataset covers roughly 30 km, representing a threefold increase

in spatial coverage. Besides, MLS point clouds are collected on the road, while PLS point clouds are collected roadside. The positional offset between them presents a challenge for PR. For related discussion, see Scan Context++ (Kim et al., 2021).

4. Benchmark

We evaluate representative PCPR methods on WHU-PCPR to illustrate the challenges it presents and expose the limitations of existing research. Specifically, we first train retrieval baselines on training sets (Hankou 1 and Hankou 2, i.e. Hankou 1&2) of WHU-PCPR, then perform retrieval and reranking on testing sets of WHU-PCPR and Oxford RobotCar (denoted as Oxford) to evaluate the baselines and analyze their sensitivity to viewpoint variations.

4.1. Experiment setting

Baselines. For retrieval, we select five representative methods as baselines. PointNetVLAD (Uy and Lee, 2018)

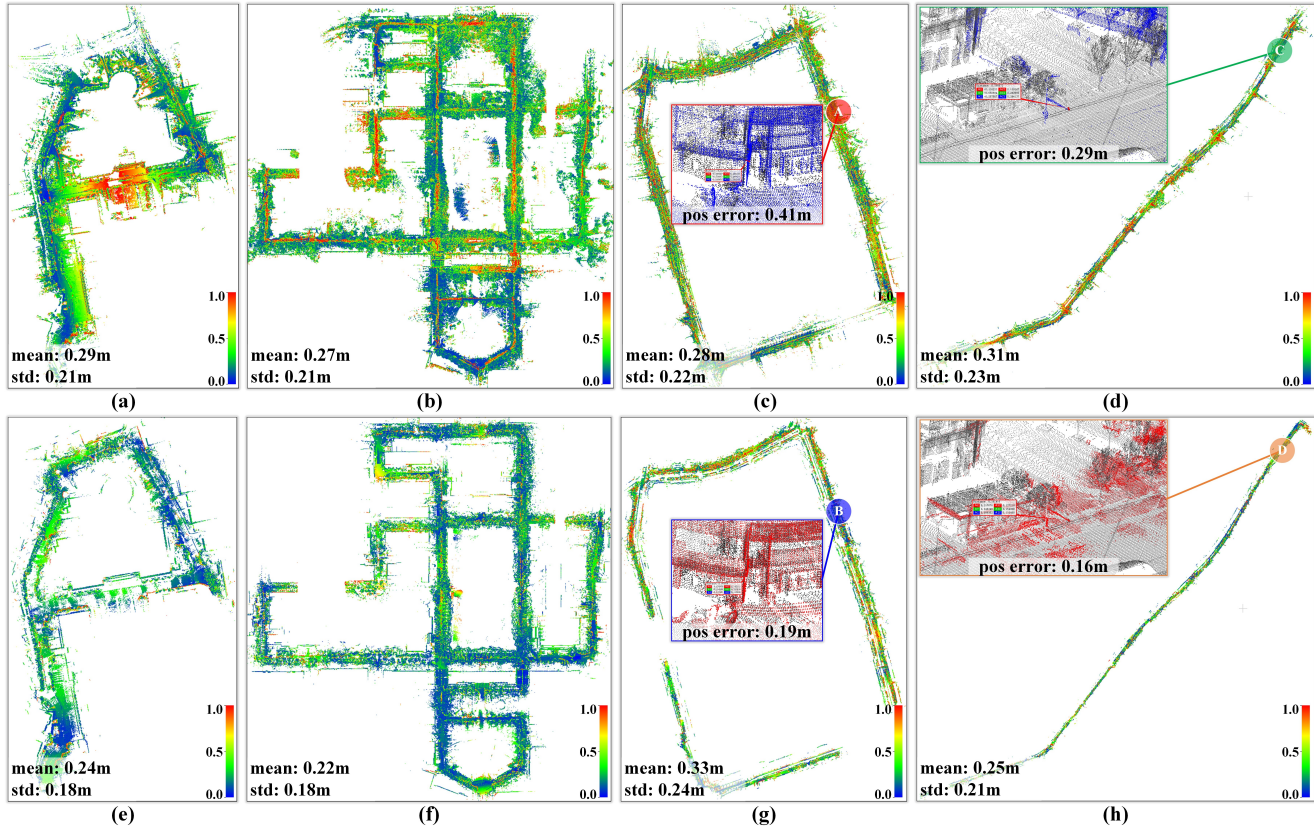


Fig. 2. Cloud to cloud distance in WHU-PCPR. (a) WHU 1&2 (CS College), (b) WHU 1&2 (Info Campus), (c) Hankou 1&2 (Zhongshan Park), (d) Hankou 1&2 (Jiefang Road 1), (e) WHU 1&3 (CS College), (f) WHU 1&3 (Info Campus), (g) Hankou 1&3 (Zhongshan Park), (h) Hankou 1&3 (Jiefang Road 1). A, B, C, and D are the positional errors of manually selected corresponding points (gray/blue/red: phase 1/2/3).

is the first DL-based PCPR method. PPTNet (Hui et al., 2021) is a point-based state-of-the-art (SOTA) method using Transformer and NetVLAD. MinkLoc3D (Komorowski, 2021) is the first voxel-based method using sparse convolution. EgoNN (Komorowski et al., 2021) extracts local feature for 6DoF relocalization on the basis of MinkLoc3D. LoGG3D-Net (Vidanapathirana et al., 2022) is a SOTA method using sparse point-voxel convolution. For reranking, we select three representative methods as baselines. AlphaQE (Radenović et al., 2018) (denoted as aQE) is a classic query expansion method. Rank-PointRetrieval (Zhang et al., 2022) (denoted as RPR) is typical reranking method based on geometric consistency. SpectralGV (Vidanapathirana et al., 2023) (denoted as SGV) is SOTA reranking method for PCPR.

Evaluation metrics. We employ *Recall@topN* (denoted as $R@N$) and *Precision@topN* (denoted as $P@N$) as quantitative metrics to evaluate PCPR performance. $R@N$ measures the ratio of successfully retrieved submaps, while $P@N$ indicates the proportion of correct results among the retrieved top N submaps. For retrieval, we report only $R@N$, especially $R@1$ and $R@1\%$. For reranking, we calculate both $R@N$ and $P@N$.

Implementation details. We primarily adopt the official implementations of all baseline methods. For retrieval, following the practice of MinkLoc3D (Komorowski, 2021), we supervise all networks using the batch hard triplet margin loss. For reranking, each point cloud submap retains 128 local features. For better performance on heterogeneous point clouds, we normalize the global features with reference to PatchAugNet (Zou et al., 2023). All retrieval baselines are implemented in PyTorch and trained on a Nvidia® RTX 3080-Ti GPU. All reranking baselines run on Intel® Core i9-14900KF CPU.

4.2. Quantitative evaluation for PCPR

4.2.1. Retrieval results

Table 3 and Fig. 4 present the retrieval results of various baselines. Overall, LoGG3D-Net, a retrieval method utilizing sparse point-voxel convolution, achieves the best performance. We analyze these evaluation results from the perspectives of generalization, viewpoint robustness, as well as efficiency.

Generalization. As shown in Table 3 and Fig. 4 (a, d), after being trained on the Hankou data from phase 1 and 2 (denoted as Hankou 1&2), the retrieval methods perform the best on Hankou 1&2, followed by WHU 1&2. Taking LoGG3D-Net as an example, it attains an $R@1$ of

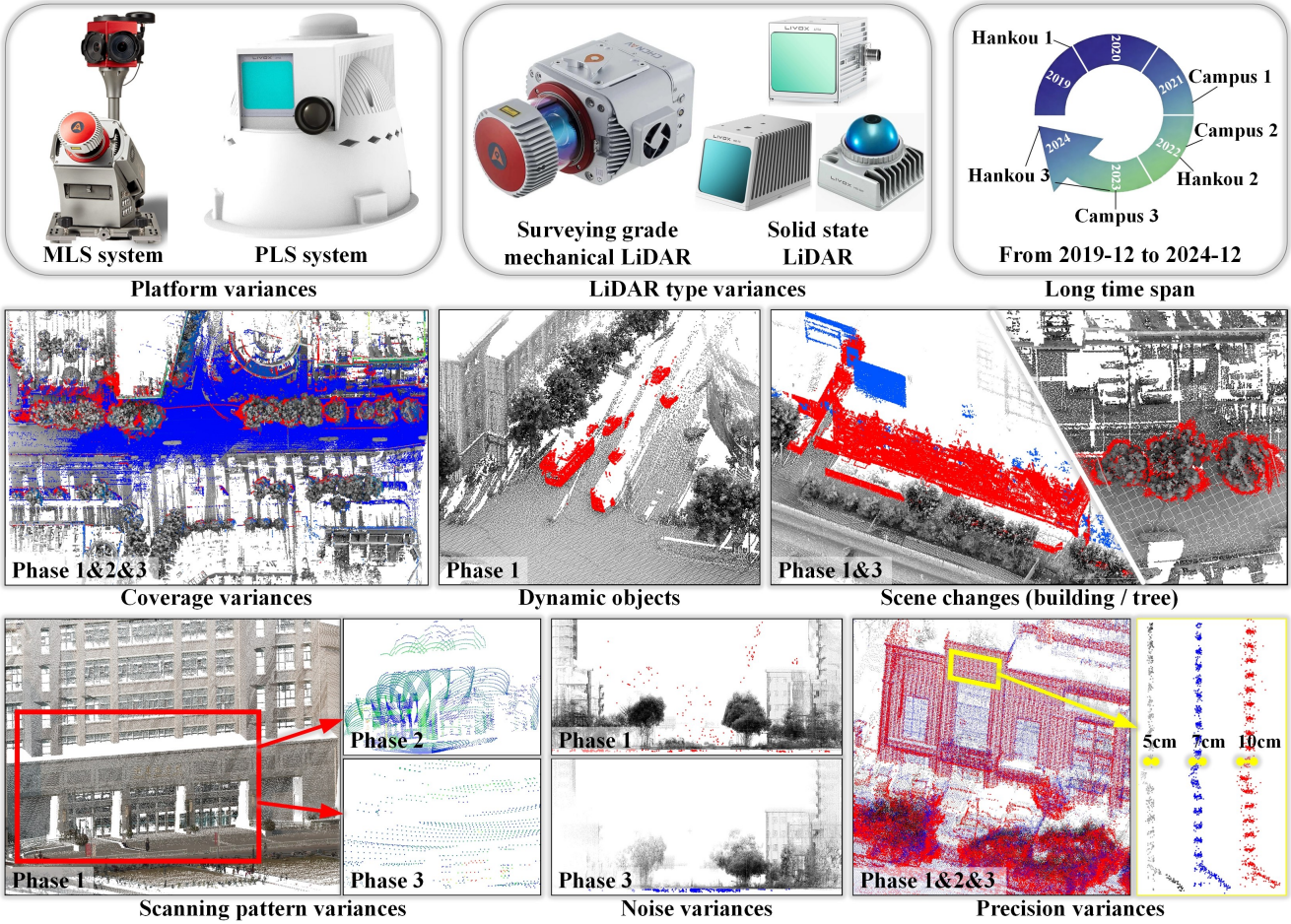


Fig. 3. Characteristics of WHU-PCPR.

80.70% and $R@1\%$ of 97.05% on Hankou 1&2. However, its performance drops significantly on WHU 1&2, with $R@1$ and $R@1\%$ falling to 40.13% and 74.71%, respectively. This decline stems from substantial differences in the shape, quantity, and distribution of surface features across scenes. Hankou road scenes are typically more open, featuring numerous high-rise buildings, elevated structures, and street trees. In contrast, WHU road scenes are characterized by dense vegetation and fewer artificial objects (see Fig. 1). However, existing methods are significantly overfitting on Hankou data, limiting their generalizability to other scenes.

As shown in Table 3 and Fig. 4 (a-c), after being trained on Hankou 1&2, the retrieval methods also exhibit a significant performance drop on Hankou 1&3 and Hankou 2&3. For example, $R@1$ and $R@1\%$ on Hankou 1&3 are only 36.25% and 70.25%, respectively, while they are 46.55% and 77.74% on Hankou 2&3.

This decline is attributed to the domain gap arising from different data acquisition systems: Phase 1 data is collected using survey-grade MLS systems, whereas phases 2 and 3 employ low-cost PLS systems with different LiDARs. This results in heterogeneous point clouds with distinct characteristics (see Fig. 3). Consequently, the methods overfit to the specific acquisition equipments of the training data,

limiting their generalizability to data from other acquisition equipments.

As shown in Table 3 and Fig. 4 (e-f), all methods face challenges from both the differences in scenes and equipments, leading to a further performance decline. Taking LoGG3D-Net as an example, $R@1$ and $R@1\%$ on WHU 1&3 are only 18.85% and 51.79%, while they are 28.36% and 68.12% on WHU 2&3. The superior performance on WHU 2&3 over WHU 1&3 indicates that the domain gap between mechanical LiDAR and solid-state LiDAR is greater than that between different solid-state LiDARs themselves. Furthermore, despite significant differences in scenes and acquisition equipments between Oxford and Hankou 1&2, LoGG3D-Net performs considerably better on Oxford than on WHU 1&2. The reason is that there is no domain gaps between query and map point clouds within Oxford itself.

Viewpoint robustness. Fig. 5 presents the PR performance of various retrieval baselines under different viewpoints. As shown, point-based and voxel-based methods like PointNetVLAD and MinkLoc3D exhibit high sensitivity to viewpoint variations. When query submaps are rotated 30 degrees around the z-axis, $R@1$ and $R@1\%$ of all methods drop below 20%. When rotating 90 degrees around the z-axis, all methods are basically unusable. The experimental

Table 3
Retrieval results on WHU-PCPR and Oxford.

Method	Hankou 1&2		Hankou 1&3		Hankou 2&3		WHU 1&2		WHU 1&3		WHU 2&3		Oxford		Average		time (ms)
	R@1	R@1%															
PointNetVLAD	32.43	64.01	7.45	20.94	15.81	36.04	45.67	72.76	9.96	29.51	18.33	42.99	74.45	88.92	29.16	50.74	2.96
PPT-Net	56.71	87.95	18.81	46.54	24.20	52.66	23.94	49.82	6.17	22.84	15.46	44.38	65.94	86.78	30.18	55.85	14.72
MinkLoc3D	64.87	94.22	29.82	62.85	40.05	73.18	24.32	54.81	11.63	36.26	18.66	53.69	60.36	84.32	35.67	65.62	4.72
EgoNN	71.43	93.68	24.69	47.00	32.50	55.92	36.39	65.38	11.82	37.49	17.51	48.01	62.50	84.04	36.69	61.65	16.29
LoGG3D-Net	80.70	97.05	36.25	70.25	46.55	77.74	40.13	74.71	18.85	51.79	28.36	68.12	68.50	88.20	45.62	75.41	19.13

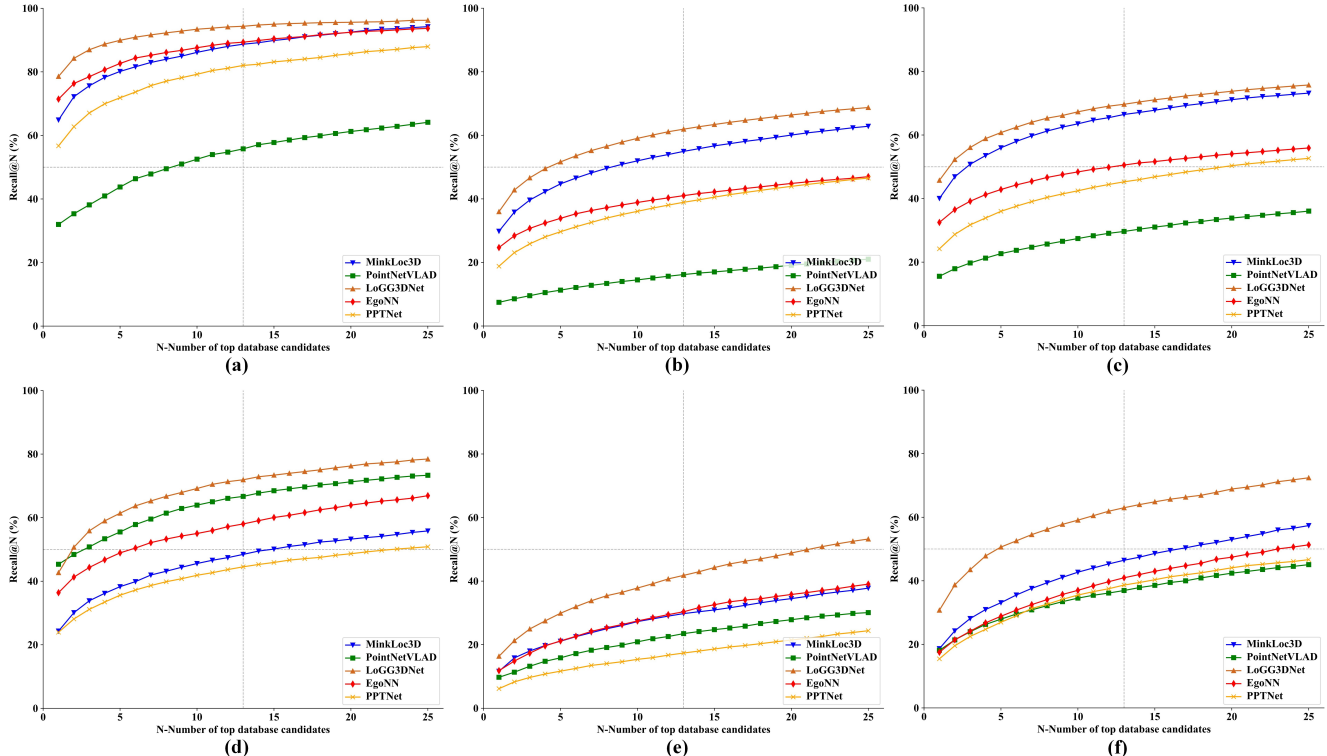


Fig. 4. Recall curves of retrieval baselines on WHU-PCPR. (a) Hankou 1&2, (b) Hankou 1&3, (c) Hankou 2&3, (d) WHU 1&2, (e) WHU 1&3, (f) WHU 2&3.

results demonstrate that viewpoint variation poses a significant challenge to PCPR tasks, and this problem cannot be solved or alleviated by reranking.

Efficiency. As shown in Table 3, baseline methods demonstrate high computational efficiency, with each retrieval time not exceeding 20 ms. Overall, voxel-based methods are less efficient than point-based ones, and LoGG3D-Net, which uses sparse point-voxel convolution, has the highest computational cost.

In summary, the diversity in scenes, collection platforms, and LiDAR types within WHU-PCPR presents substantial challenges for PCPR, and there is significant room for improvement in the performance of all retrieval baselines. Thus, WHU-PCPR is valuable for advancing research toward robust PCPR methods that generalize across varying scenes, platforms, and LiDAR types.

4.2.2. Reranking results

Table 4, Fig. 6, and Fig. 7 presents the results of reranking baselines. Overall, geometric consistency-based reranking method SGV achieves the best performance, while other reranking methods offer only marginal improvements. We analyze these evaluation results from the perspectives of the impacts of different retrieval methods and scenes, as well as computational efficiency.

Impacts of different retrieval methods on reranking.

As shown in Table 4, when PPTNet is used for initial retrieval, even the top-performing reranking method SGV yields no performance improvement. In contrast, when superior retrieval methods such as EgoNN and LoGG3D-Net are employed for initial retrieval, SGV significantly enhances the PR performance, with improvements of up to 12.17% in $R@1$, 8.49% in $R@5$, and 7.55% in $P@5$. The experimental results indicate that: 1) built upon high-performing retrieval methods, reranking methods based on geometry consistency can substantially enhance final performance; 2)

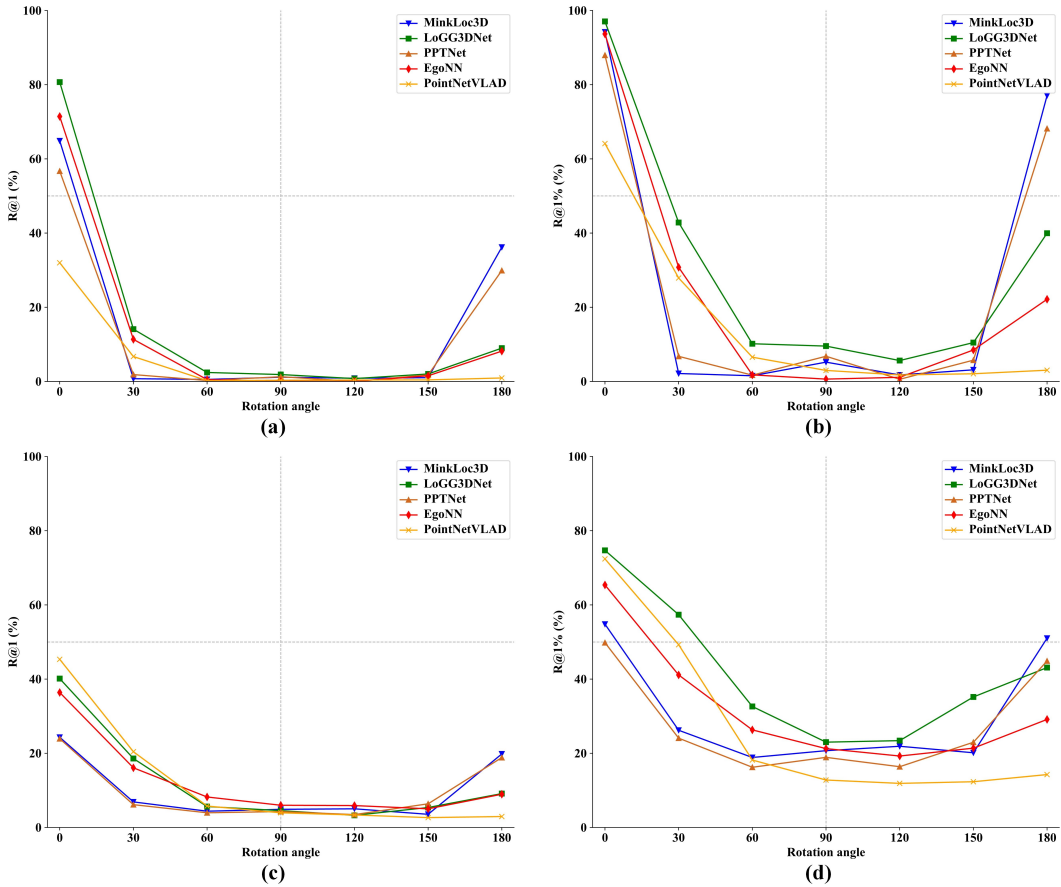


Fig. 5. Retrieval results of various baselines with different viewpoints. (a) $R@1$ on Hankou 1&2, (b) $R@1\%$ on Hankou 1&2, (c) $R@1$ on WHU 1&2, (d) $R@1\%$ on WHU 1&2.

the effectiveness of reranking is highly dependent on initial retrieval methods. This is because methods like EgoNN and LoGG3D-Net possess stronger feature extraction capabilities, producing more discriminative local features which are a prerequisite for the effectiveness of reranking methods based on geometric consistency.

Impacts of different scenes and equipments on reranking. As shown in Table 4, when using LoGG3D-Net for initial retrieval and SGV for reranking, $R@1$ increases by 7.44%, 10.12%, 3.79%, 3.69%, and 12.17% respectively on Hankou 1&2, Hankou 1&3, WHU 1&2, WHU 1&3, and WHU 2&3, and $P@5$ increased by 7.23%, 6.09%, 1.49%, 1.81%, and 7.55% respectively. The improvement in performance of SGV varies across different datasets, with the greatest improvement observed on WHU 2&3, although it differs from the training set's scenes and acquisition equipments.

Efficiency. As shown in the last column of Table 4, the query expansion achieves the highest computational efficiency, while RPR essentially achieves reranking by evaluating the results of point cloud registration, with the lowest efficiency. Meanwhile, the runtime of SGV remains consistently within 5 ms.

PCPR cases. Fig. 7 presents three successful cases of using LoGG3D-Net for retrieval and SGV for reranking. In

these cases, the main scenes of query submaps are trees, with few artificial objects, causing LoGG3D-Net to return an incorrect top-1 candidate initially. SGV utilizes local features extracted by LoGG3D-Net and adjusts the initial retrieval results through spectral matching scores, effectively improving the PR performance.

Fig. 8 presents PR bad cases using LoGG3D-Net and SGV. The three failure cases illustrate distinct challenges: Case 1 lacks sufficient features due to vegetation-only scenes and typically occurs in forested areas. Case 2 is characterized by low distinctiveness at wide intersections, and this situation more prevalent in urban areas due to constraints imposed by the submap radius. Case 3 is misled by coincidental scene similarities in the map and has a higher probability of occurring in urban settings, necessitating the use of coarse localization technology. All are common corner cases where single-shot PCPR typically fails.

In summary, certain reranking methods can significantly enhance the PR performance on our challenging dataset. Among them, SGV, a reranking method based on geometric consistency, represents the current SOTA. However, research in this direction remains nascent, indicating substantial potential for future development.

Table 4

Rerank results on WHU-PCPR.

Rerank method	Retrieval method	Hankou 1&2		Hankou 1&3		Hankou 2&3		WHU 1&2		WHU 1&3		WHU 2&3		time (ms)
		R@1	R@5/P@5	R@1	R@5/P@5	R@1	R@5/P@5	R@1	R@5/P@5	R@1	R@5/P@5	R@1	R@5/P@5	
None	PPTNet	56.71	71.85/54.50	18.81	29.67/18.00	24.20	36.00/23.52	23.94	35.60/23.11	6.17	11.67/5.87	15.46	26.96/14.87	-
	LoGG3D-Net	80.70	91.82/76.65	36.25	52.93/33.94	46.55	62.60/44.06	40.13	58.50/36.94	18.85	32.45/16.46	28.36	47.53/25.52	-
	EgoNN	71.43	82.65/69.57	24.69	33.88/24.02	32.50	42.86/31.50	36.39	48.92/34.75	11.82	21.19/12.19	17.51	28.85/17.07	-
aQE	PPTNet	53.97	64.45/51.58	16.77	23.03/16.44	17.74	23.83/17.56	18.03	23.53/17.84	4.65	7.53/4.63	14.56	22.81/14.23	0.27
	LoGG3D-Net	72.79	82.72/71.55	31.41	41.38/30.82	31.92	40.54/31.39	30.42	40.73/29.76	14.25	21.99/13.94	24.41	38.85/24.01	0.23
	EgoNN	63.13	73.59/61.82	21.78	27.44/21.64	23.09	29.01/22.66	26.58	32.41/25.80	11.08	15.83/10.91	16.39	24.35/16.42	0.27
SGV	PPTNet	51.44	78.51/47.76	16.41	32.00/15.24	18.78	31.73/17.23	17.32	31.44/16.87	4.93	12.63/4.73	14.81	30.94/13.71	5.32
	LoGG3D-Net	88.14	94.76/83.88	46.37	57.92/40.03	46.48	52.98/41.19	43.92	54.48/38.43	22.54	34.23/18.27	40.53	56.02/33.07	2.88
	EgoNN	89.33	92.25/85.11	35.65	40.72/31.05	36.87	40.04/32.39	42.85	50.53/37.40	22.05	28.78/17.48	32.58	41.92/26.58	3.82
RPR	PPTNet	56.71	71.85/54.50	17.31	27.37/16.55	17.94	27.02/17.41	19.83	29.31/19.14	5.34	10.06/5.08	14.87	25.93/14.30	290.09
	LoGG3D-Net	78.86	91.85/73.62	32.65	48.00/30.21	33.56	45.48/30.96	33.05	47.94/30.23	16.23	28.46/14.48	27.04	45.96/24.30	64.81
	EgoNN	71.43	82.65/69.57	22.71	31.22/22.07	24.24	32.38/23.39	30.02	40.14/28.66	10.40	18.57/10.75	16.86	27.75/16.41	106.39

5. Challenges and research directions

PCPR mainly faces challenges such as generalization, scene changes, and viewpoint variations, and future research will mainly focus on these challenges:

Generalization. During long-term operation, localization systems often necessitate continuous operation across diverse scenes using varied data acquisition platforms. Point clouds collected by different equipments in different scenes has significant differences in scene characteristics, coverage, scanning pattern, density, accuracy, and noise level, namely domain gaps. These gaps are particularly salient in WHU-PCPR (see Fig. 1 and 3). Although recent methods like PatchAugNet (Zou et al., 2023) and HeLiOS (Jung et al., 2025a) attempt to improve adaptability to domain gaps through self-supervised auxiliary tasks and overlap-based data mining, the generalization of existing PCPR methods remains limited and cannot be transferred to different scenes and equipments. In the future, we can transfer prior knowledge from visual models (Jung et al., 2025b) and introduce domain adaptation and domain generalization (Qiao et al., 2020) to PCPR tasks.

Scene changes. Localization scenes typically evolve dynamically over time, including real-time changes from objects like pedestrians and vehicles, as well as long-term changes of buildings, trees, and other land features. WHU-PCPR contains abundant examples of scenes undergoing both types of changes (see Fig. 3). For real-time changes, methods like Octomap (Hornung et al., 2013) can often be employed to filter out dynamic objects. For long-term changes, retrieving the correct places becomes challenging when relying solely on the limited information contained in one point cloud, especially if the scene alterations are substantial. Usually, the robustness of PR and localization can be improved by leveraging sequential information from continuously collected point clouds (Ma et al., 2022) or applying point cloud registration to identify retrieval failures and significant scene changes (Kirsch et al., 2022).

Viewpoint variations. When a localization system passes through the same place multiple times, significant viewpoint variations may occur, presenting a formidable challenge to PCPR. Recent methods like RPR-Net (Fan

et al., 2023) and RIA-Net (Hao et al., 2024) have enhanced robustness to viewpoint variations by augmenting low-level rotation-invariant features. Meanwhile, approaches like OverlapTransformer (Ma et al., 2022) extract rotation-invariant features from range images using Transformer architectures. In summary, relevant research remains at an early stage, and WHU-PCPR can provide effective data support for such studies.

Pose estimation. PR determines only a coarse location within the map, with accuracy limited by the density of map submaps. To enhance precision, it is often combined with pose estimation techniques such as point cloud registration. First, since PR utilizes global features while pose estimation relies on local features, extracting both simultaneously improves localization efficiency (Cattaneo et al., 2022). Second, Monte Carlo localization can be integrated to achieve robust localization by leveraging sequential point clouds. Key challenges lie in ensuring reliable initialization and detecting localization failures (Zou et al., 2025).

6. Conclusion

This paper establishes WHU-PCPR, a cross-platform heterogeneous point cloud dataset for PR. The main features of this dataset are threefold. 1) Cross-platform heterogeneous point clouds: Phase 1 is captured using survey-grade MLS systems equipped with a mechanical LiDAR, while Phases 2 and 3 are captured using low-cost, portable PLS systems equipped with a solid-state LiDAR. The multi-phase point cloud data exhibits significant domain gaps. 2) Complex localization scenes: The Hankou and WHU scenes differ substantially in the shape, quantity, and distribution of objects. Furthermore, data collection spans 60 months across three phases, introducing both real-time and long-term scene changes. 3) Large-scale spatial coverage: The dataset's total trajectory length is 82.3 km, with a non-repetitive collected trajectory length of approximately 30 km, far exceeding the scale of widely used datasets like Oxford RobotCar. Based on WHU-PCPR, this paper evaluates several representative PCPR methods. Experimental results reveal two main findings. Existing retrieval methods show considerable room for improvement in generalizing across

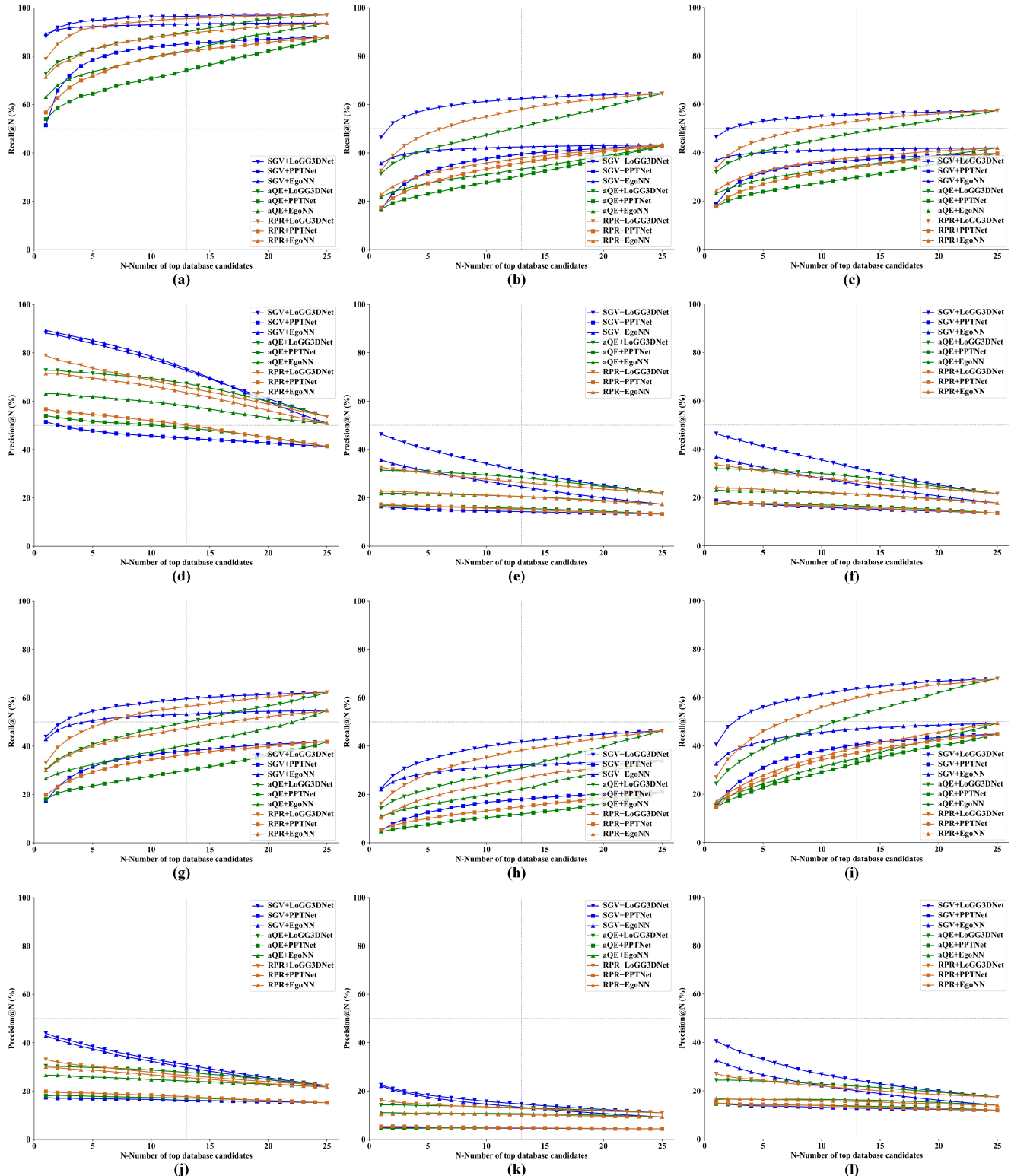


Fig. 6. Recall and precision curves of reranking baselines on WHU-PCPR. (a)/(d) Hankou 1&2, (b)/(e) Hankou 1&3, (c)/(f) Hankou 2&3, (g)/(j) WHU 1&2, (h)/(k) WHU 1&3, (i)/(l) WHU 2&3.

domains and handling viewpoint variations. While reranking can effectively enhance initial retrieval results, research in this area remains limited. Future work should therefore focus on improving generalization and robustness to scene changes

and viewpoint variations. By introducing WHU-PCPR, this paper aims to address the limitations of existing datasets and advance the frontier of PCPR tasks towards more complex

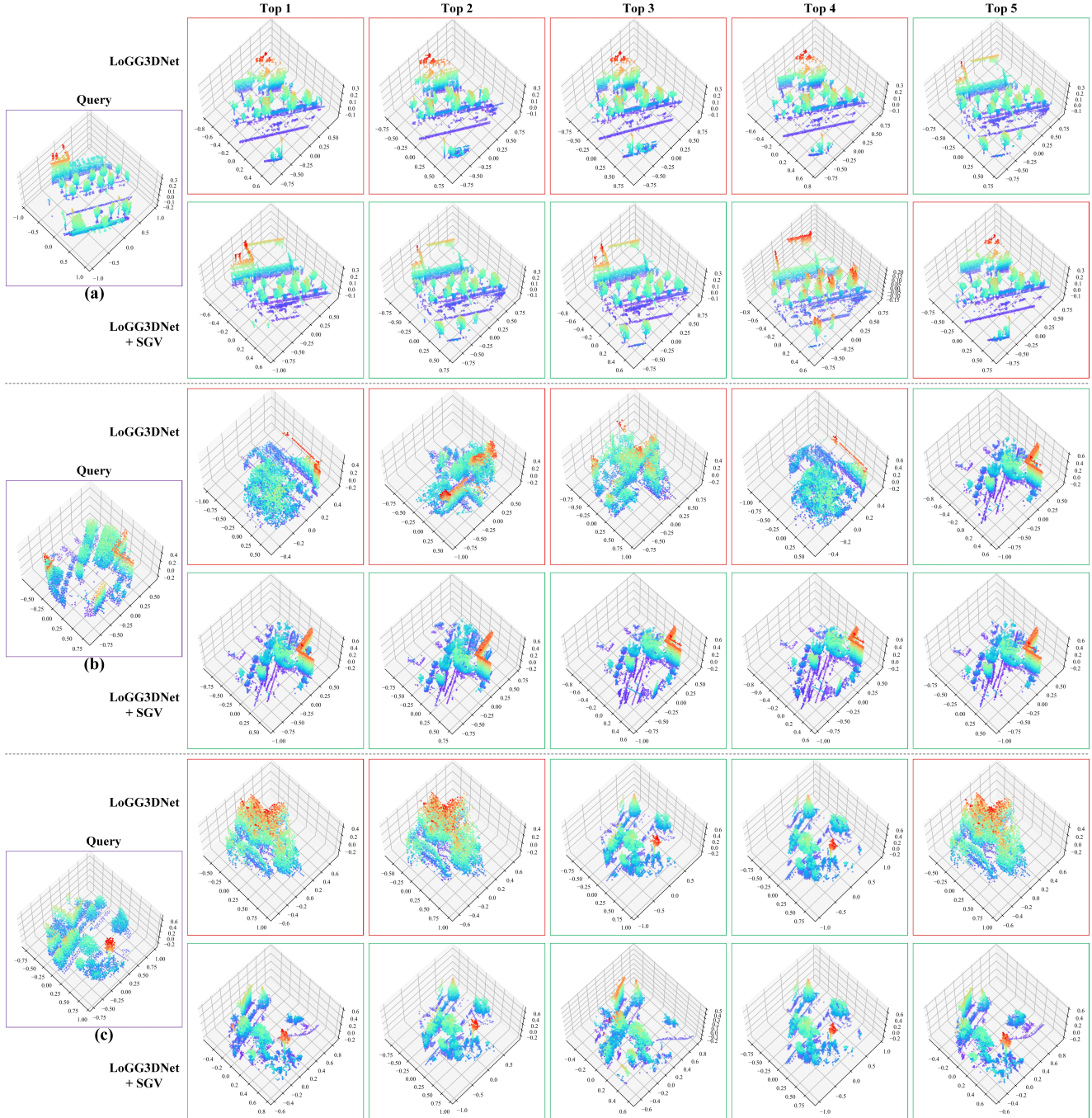


Fig. 7. Success PR cases when using LoGG3DNet for retrieval and SGV for reranking. (a) case 1 on Hankou, (b) case 2 on WHU, (c) case 3 on WHU. Purple represents query, red represents failure, and green represents success.

and diverse urban environments, thereby enhancing the practicality of PCPR approaches.

CRediT authorship contribution statement

Xianghong Zou: Writing – review & editing, Writing – original draft, Visualization, Methodology, Investigation. **Jianping Li:** Writing – review & editing, Resources, Project administration. **Yandi Yang:** Writing – review & editing. **Weitong Wu:** Writing – review & editing. **Yuan Wang:**

Writing – review & editing. **Qiegen Liu:** Writing – review & editing, Resources, Project administration. **Zhen Dong:** Writing – review & editing, Resources, Project administration.

7. Declaration of interests

The authors declare that they have no known competing financial interests or personal relationships that could have appeared to influence the work reported in this paper.

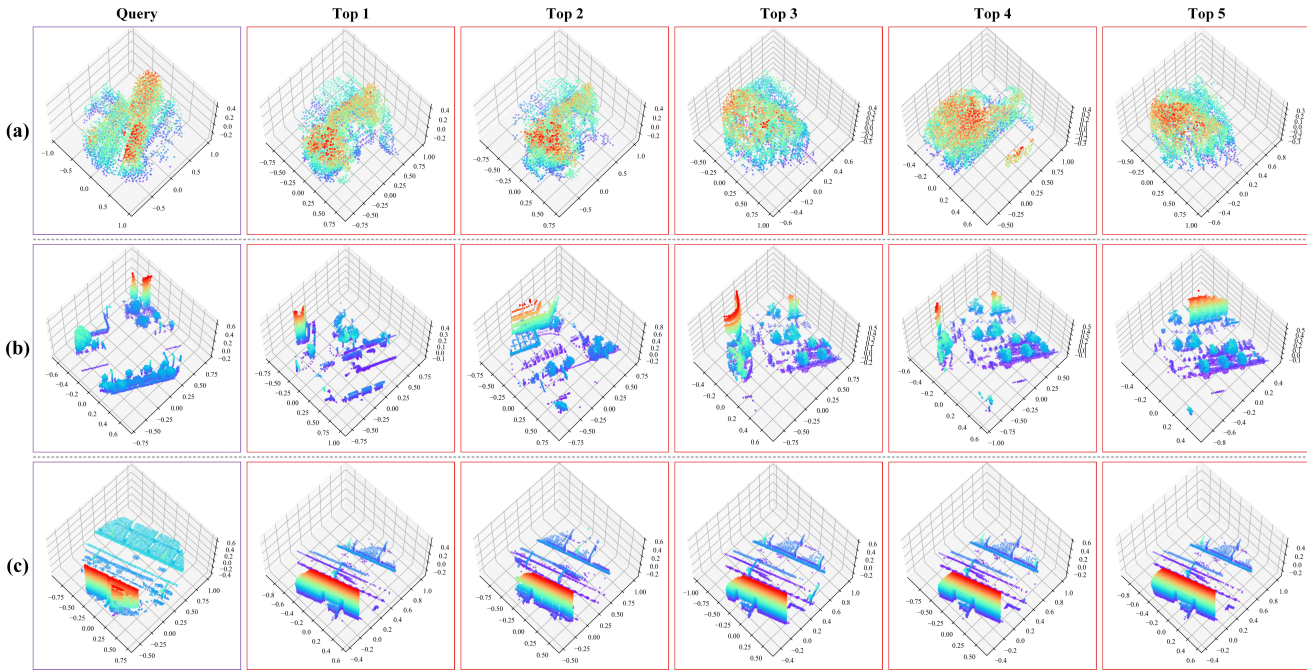


Fig. 8. Bad cases of place recognition (LoGG3DNet and SGV) on WHU-PCPR. (a) case 1, (b) case 2, (c) case 3.

References

Häne, C., Heng, L., Lee, G.H., Fraundorfer, F., Furgale, P., Sattler, T., Pollefeys, M., 2017. 3d visual perception for self-driving cars using a multi-camera system: Calibration, mapping, localization, and obstacle detection. *Image and Vision Computing* 68, 14–27.

Wang, X., Mizukami, Y., Tada, M., Matsuno, F., 2021. Navigation of a mobile robot in a dynamic environment using a point cloud map. *Artificial Life and Robotics* 26, 10–20.

Li, J., Xu, X., Liu, J., Cao, K., Yuan, S., Xie, L., 2025. Ua-mpc: Uncertainty-aware model predictive control for motorized lidar odometry. *IEEE Robotics and Automation Letters*.

Yuan, J., Zhang, J., Ding, S., Dong, X., 2017. Cooperative localization for disconnected sensor networks and a mobile robot in friendly environments. *Information Fusion* 37, 22–36.

Li, J., Nguyen, T.M., Cao, M., Yuan, S., Hung, T.Y., Xie, L., 2025. Graph optimality-aware stochastic lidar bundle adjustment with progressive spatial smoothing. *IEEE Transactions on Intelligent Transportation Systems*.

Kim, G., Kim, A., 2020. Remove, then revert: Static point cloud map construction using multiresolution range images, in: 2020 IEEE/RSJ International Conference on Intelligent Robots and Systems (IROS), IEEE, pp. 10758–10765.

Chi, H.L., Kim, M.K., Liu, K.Z., Thedja, J., Seo, J., Lee, D.E., 2022. Rebar inspection integrating augmented reality and laser scanning. *Automation in Construction* 136, 104183.

Bin Shamsudin, A.U., Mizuno, N., Fujita, J., Ohno, K., Hamada, R., Westfchel, T., Tadokoro, S., Amano, H., 2017. Evaluation of lidar and gps based slam on fire disaster in petrochemical complexes, in: 2017 IEEE International Symposium on Safety, Security and Rescue Robotics (SSRR), pp. 48–54.

Li, J., Yang, B., Chen, C., Habib, A., 2019. Nrli-uav: Non-rigid registration of sequential raw laser scans and images for low-cost uav lidar point cloud quality improvement. *ISPRS Journal of Photogrammetry and Remote Sensing* 158, 123–145.

Yang, B., Dong, Z., Liang, F., Mi, X., 2024. Ubiquitous Point Cloud: Theory, Model, and Applications. CRC Press.

Zou, X., Li, J., Wang, Y., Liang, F., Wu, W., Wang, H., Yang, B., Dong, Z., 2023. Patchaugnet: Patch feature augmentation-based heterogeneous point cloud place recognition in large-scale street scenes. *ISPRS Journal of Photogrammetry and Remote Sensing* 206, 273–292.

Qingqing, L., Xianjia, Y., Queralta, J.P., Westerlund, T., 2022. Multi-modal lidar dataset for benchmarking general-purpose localization and mapping algorithms, in: 2022 IEEE/RSJ International Conference on Intelligent Robots and Systems (IROS), IEEE, pp. 3837–3844.

Li, J., Wu, W., Yang, B., Zou, X., Yang, Y., Zhao, X., Dong, Z., 2023. Whu-helmet: A helmet-based multisensor slam dataset for the evaluation of real-time 3-d mapping in large-scale gnss-denied environments. *IEEE Transactions on Geoscience and Remote Sensing* 61, 1–16.

Li, J., Yuan, S., Cao, M., Nguyen, T.M., Cao, K., Xie, L., 2024. Hcto: Optimality-aware lidar inertial odometry with hybrid continuous time optimization for compact wearable mapping system. *ISPRS Journal of Photogrammetry and Remote Sensing* 211, 228–243. URL: <https://www.sciencedirect.com/science/article/pii/S092427162400162X>, doi:<https://doi.org/10.1016/j.isprsjprs.2024.04.004>.

Li, J., Xu, X., Liu, Z., Yuan, S., Cao, M., Xie, L., 2026. Aeos: Active environment-aware optimal scanning control for uav lidar-inertial odometry in complex scenes. *ISPRS Journal of Photogrammetry and Remote Sensing* 232, 476–491.

Kim, G., Kim, A., 2018. Scan context: Egocentric spatial descriptor for place recognition within 3d point cloud map, in: 2018 IEEE/RSJ International Conference on Intelligent Robots and Systems (IROS), pp. 4802–4809.

He, L., Wang, X., Zhang, H., 2016. M2dp: A novel 3d point cloud descriptor and its application in loop closure detection, in: 2016 IEEE/RSJ International Conference on Intelligent Robots and Systems (IROS), pp. 231–237.

Hui, L., Yang, H., Cheng, M., Xie, J., Yang, J., 2021. Pyramid point cloud transformer for large-scale place recognition, in: Proceedings of the IEEE/CVF International Conference on Computer Vision, pp. 6098–6107.

Komorowski, J., 2021. Minkloc3d: Point cloud based large-scale place recognition, in: Proceedings of the IEEE/CVF Winter Conference on Applications of Computer Vision, pp. 1790–1799.

Zhang, Y., Shi, P., Li, J., 2024. Lidar-based place recognition for autonomous driving: A survey. *ACM Computing Surveys* 57, 1–36.

Zhang, W., Zhou, H., Dong, Z., Yan, Q., Xiao, C., 2022. Rank-pointretrieval: Reranking point cloud retrieval via a visually consistent registration evaluation. *IEEE Transactions on Visualization and Computer Graphics*.

Vidanapathirana, K., Moghadam, P., Sridharan, S., Fookes, C., 2023. Spectral geometric verification: Re-ranking point cloud retrieval for metric localization. *IEEE Robotics and Automation Letters* 8, 2494–2501.

Barnes, D., Gadd, M., Murcutt, P., Newman, P., Posner, I., 2020. The oxford radar robotcar dataset: A radar extension to the oxford robotcar dataset, in: 2020 IEEE international conference on robotics and automation (ICRA), pp. 6433–6438.

Geiger, A., Lenz, P., Urtasun, R., 2012. Are we ready for autonomous driving? the kitti vision benchmark suite, in: 2012 IEEE conference on computer vision and pattern recognition, pp. 3354–3361.

Jung, M., Yang, W., Lee, D., Gil, H., Kim, G., Kim, A., 2023. Helipr: Heterogeneous lidar dataset for inter-lidar place recognition under spatiotemporal variations. *The International Journal of Robotics Research* , 02783649241242136.

Carlevaris-Bianco, N., Ushani, A.K., Eustice, R.M., 2016. University of michigan north campus long-term vision and lidar dataset. *The International Journal of Robotics Research* 35, 1023–1035.

Knights, J., Vidanapathirana, K., Ramezani, M., Sridharan, S., Fookes, C., Moghadam, P., 2023. Wild-places: A large-scale dataset for lidar place recognition in unstructured natural environments, in: 2023 IEEE international conference on robotics and automation (ICRA), pp. 11322–11328.

Maddern, W., Pascoe, G., Linegar, C., Newman, P., 2017. 1 year, 1000 km: The oxford robotcar dataset. *The International Journal of Robotics Research* 36, 3–15.

Pandey, G., McBride, J.R., Eustice, R.M., 2011. Ford campus vision and lidar data set. *The International Journal of Robotics Research* 30, 1543–1552.

Uy, M.A., Lee, G.H., 2018. Pointnetvlad: Deep point cloud based retrieval for large-scale place recognition, in: Proceedings of the IEEE conference on computer vision and pattern recognition, pp. 4470–4479.

Lu, W., Zhou, Y., Wan, G., Hou, S., Song, S., 2019. L3-net: Towards learning based lidar localization for autonomous driving, in: Proceedings of the IEEE/CVF Conference on Computer Vision and Pattern Recognition, pp. 6389–6398.

Lin, J., Zhang, F., 2019. A fast, complete, point cloud based loop closure for lidar odometry and mapping. *arXiv preprint arXiv:1909.11811* .

Jeong, J., Cho, Y., Shin, Y.S., Roh, H., Kim, A., 2019. Complex urban dataset with multi-level sensors from highly diverse urban environments. *The International Journal of Robotics Research* 38, 642–657.

Kim, G., Park, Y.S., Cho, Y., Jeong, J., Kim, A., 2020. Mulran: Multimodal range dataset for urban place recognition, in: 2020 IEEE International Conference on Robotics and Automation (ICRA), pp. 6246–6253.

Agarwal, S., Vora, A., Pandey, G., Williams, W., Kourous, H., McBride, J., 2020. Ford multi-av seasonal dataset. *The International Journal of Robotics Research* 39, 1367–1376.

Zhou, W., Berrio, J.S., De Alvis, C., Shan, M., Worrall, S., Ward, J., Nebot, E., 2020. Developing and testing robust autonomy: The university of sydney campus data set. *IEEE Intelligent Transportation Systems Magazine* 12, 23–40.

Yin, P., Zhao, S., Ge, R., Cisneros, I., Fu, R., Zhang, J., Choset, H., Scherer, S., 2022. Alita: A large-scale incremental dataset for long-term autonomy. *arXiv preprint arXiv:2205.10737* .

Liao, Y., Xie, J., Geiger, A., 2022. Kitti-360: A novel dataset and benchmarks for urban scene understanding in 2d and 3d. *IEEE Transactions on Pattern Analysis and Machine Intelligence* 45, 3292–3310.

Ma, J., Zhang, J., Xu, J., Ai, R., Gu, W., Chen, X., 2022. Overlaptransformer: An efficient and yaw-angle-invariant transformer network for lidar-based place recognition. *IEEE Robotics and Automation Letters* 7, 6958–6965.

Burnett, K., Yoon, D.J., Wu, Y., Li, A.Z., Zhang, H., Lu, S., Qian, J., Tseng, W.K., Lambert, A., Leung, K.Y., et al., 2023. Boreas: A multi-season autonomous driving dataset. *The International Journal of Robotics Research* 42, 33–42.

Chung, D., Kim, J., Lee, C., Kim, J., 2023. Pohang canal dataset: A multimodal maritime dataset for autonomous navigation in restricted waters. *The International Journal of Robotics Research* 42, 1104–1114.

Chum, O., Philbin, J., Sivic, J., Isard, M., Zisserman, A., 2007. Total recall: Automatic query expansion with a generative feature model for object retrieval, in: 2007 IEEE 11th International Conference on Computer Vision, pp. 1–8.

Liang, F., Yang, B., Dong, Z., Huang, R., Zang, Y., Pan, Y., 2020. A novel skyline context descriptor for rapid localization of terrestrial laser scans to airborne laser scanning point clouds. *ISPRS Journal of Photogrammetry and Remote Sensing* 165, 120–132.

Xu, D., Liu, J., Hyppä, J., Liang, Y., Tao, W., 2022. A heterogeneous 3d map-based place recognition solution using virtual lidar and a polar grid height coding image descriptor. *ISPRS Journal of Photogrammetry and Remote Sensing* 183, 1–18.

Cop, K.P., Borges, P.V., Dubé, R., 2018. Delight: An efficient descriptor for global localisation using lidar intensities, in: 2018 IEEE International Conference on Robotics and Automation (ICRA), pp. 3653–3660.

Magnusson, M., Andreasson, H., Nüchter, A., Lilienthal, A.J., 2009. Automatic appearance-based loop detection from three-dimensional laser data using the normal distributions transform. *Journal of Field Robotics* 26, 892–914.

Röhling, T., Mack, J., Schulz, D., 2015. A fast histogram-based similarity measure for detecting loop closures in 3-d lidar data, in: 2015 IEEE/RSJ international conference on intelligent robots and systems (IROS), pp. 736–741.

Bosse, M., Zlot, R., 2013. Place recognition using keypoint voting in large 3d lidar datasets, in: 2013 IEEE international conference on robotics and automation, pp. 2677–2684.

Dubé, R., Dugas, D., Stumm, E., Nieto, J., Siegwart, R., Cadena, C., 2017. Segmatch: Segment based place recognition in 3d point clouds, in: 2017 IEEE International Conference on Robotics and Automation (ICRA), pp. 5266–5272.

Qi, C.R., Su, H., Mo, K., Guibas, L.J., 2017. Pointnet: Deep learning on point sets for 3d classification and segmentation, in: Proceedings of the IEEE conference on computer vision and pattern recognition, pp. 652–660.

Xie, Y., Wang, B., Wang, H., Liang, F., Zhang, W., Dong, Z., Yang, B., 2024. Look at the whole scene: General point cloud place recognition by classification proxy. *ISPRS Journal of Photogrammetry and Remote Sensing* 215, 15–30.

Radenović, F., Tolias, G., Chum, O., 2018. Fine-tuning cnn image retrieval with no human annotation. *IEEE transactions on pattern analysis and machine intelligence* 41, 1655–1668.

Komorowski, J., Wysoczanska, M., Trzciński, T., 2021. Egonn: Egocentric neural network for point cloud based 6dof relocalization at the city scale. *IEEE Robotics and Automation Letters* 7, 722–729.

Vidanapathirana, K., Ramezani, M., Moghadam, P., Sridharan, S., Fookes, C., 2022. Logg3d-net: Locally guided global descriptor learning for 3d place recognition, in: 2022 International Conference on Robotics and Automation (ICRA), pp. 2215–2221.

Chen, X., Läbe, T., Milioto, A., Röhling, T., Vysotska, O., Haag, A., Behley, J., Stachniss, C., 2021. Overlapnet: Loop closing for lidar-based slam. *arXiv preprint arXiv:2105.11344* .

Kim, G., Park, B., Kim, A., 2019. 1-day learning, 1-year localization: Long-term lidar localization using scan context image. *IEEE Robotics and Automation Letters* 4, 1948–1955.

Luo, L., Zheng, S., Li, Y., Fan, Y., Yu, B., Cao, S.Y., Li, J., Shen, H.L., 2023. Bevplace: Learning lidar-based place recognition using bird's eye view images, in: Proceedings of the IEEE/CVF International Conference on Computer Vision, pp. 8700–8709.

Joshi, M.D., Deshmukh, R.M., Hemke, K.N., Bhake, A., Wajgi, R., 2014. Image retrieval and re-ranking techniques-a survey. *Signal and Image Processing: An International Journal (SIPIJ)* 5.

Tolias, G., Sicre, R., Jégou, H., 2015. Particular object retrieval with integral max-pooling of cnn activations. *arXiv preprint arXiv:1511.05879* .

Bai, S., Bai, X., Zhou, Z., Zhang, Z., Tian, Q., Latecki, L.J., 2017. Gift: Towards scalable 3d shape retrieval. *IEEE Transactions on Multimedia* 19, 1257–1271.

Xu, W., Cai, Y., He, D., Lin, J., Zhang, F., 2022. Fast-lio2: Fast direct lidar-inertial odometry. *IEEE Transactions on Robotics* 38, 2053–2073.

Hornung, A., Wurm, K.M., Bennewitz, M., Stachniss, C., Burgard, W., 2013. Octomap: an efficient probabilistic 3d mapping framework based on octrees. Springer US .

Zhang, W., Qi, J., Wan, P., Wang, H., Yan, G., 2016. An easy-to-use airborne lidar data filtering method based on cloth simulation. *Remote Sensing* 8, 501.

Kim, G., Choi, S., Kim, A., 2021. Scan context++: Structural place recognition robust to rotation and lateral variations in urban environments. *IEEE Transactions on Robotics* 38, 1856–1874.

Jung, M., Jung, S., Gil, H., Kim, A., 2025a. Helios: Heterogeneous lidar place recognition via overlap-based learning and local spherical transformer.

Jung, M., Fu, L.F.T., Fallon, M., Kim, A., 2025b. Imlpr: Image-based lidar place recognition using vision foundation models .

Qiao, Z., Hu, H., Chen, S., Liu, Z., Wang, H., 2020. vlpd-net: A registration-aided domain adaptation network for 3d point cloud based place recognition .

Ma, J., Chen, X., Xu, J., Xiong, G., 2022. Seqot: A spatial-temporal transformer network for place recognition using sequential lidar data. *IEEE Transactions on Industrial Electronics* 70, 8225–8234.

Kirsch, A., Günter, A., König, M., 2022. Predicting alignability of point cloud pairs for point cloud registration using features, in: 2022 12th International Conference on Pattern Recognition Systems (ICPRS), pp. 1–6. doi:10.1109/ICPRS54038.2022.9854071.

Fan, Z., Song, Z., Zhang, W., Liu, H., He, J., Du, X., 2023. Rpr-net: A point cloud-based rotation-aware large scale place recognition network. *Lecture Notes in Computer Science* , 709–725.

Hao, W., Zhang, W., Su, H., 2024. Ria-net: Rotation invariant aware 3d point cloud for large-scale place recognition. *IEEE robotics and automation letters* , 9.

Cattaneo, D., Vaghi, M., Valada, A., 2022. Lcdnet: Deep loop closure detection and point cloud registration for lidar slam. *IEEE Transactions on Robotics* 38, 2074–2093.

Zou, X., Li, J., Wu, W., Liang, F., Yang, B., Dong, Z., 2025. Reliable-loc: Robust sequential lidar global localization in large-scale street scenes based on verifiable cues. *ISPRS Journal of Photogrammetry and Remote Sensing* 224, 287–301.